



# Using Fourier Transform Infrared spectroscopy to produce high-resolution centennial records of past high-intensity fires from organic-rich sediment deposits

Rebecca Ryan<sup>A,\*</sup>, Anthony Dosseto<sup>A,B</sup>, Pavel Dlapa<sup>C</sup>, Zoë Thomas<sup>D,E</sup>, Ivan Simkovic<sup>C</sup>, Scott Mooney<sup>F</sup>

For full list of author affiliations and declarations see end of paper

#### \*Correspondence to:

Rebecca Ryan Wollongong Isotope Geochronology Laboratory, School of Earth, Atmospheric and Life Sciences, University of Wollongong, NSW 2522, Australia Email: rjr072@uowmail.edu.au

**Received:** 26 October 2023 **Accepted:** 2 December 2024 **Published:** 10 January 2025

Cite this: Ryan R et al. (2025) Using Fourier Transform Infrared spectroscopy to produce high-resolution centennial records of past high-intensity fires from organic-rich sediment deposits. International Journal of Wildland Fire 34, WF23175. doi:10.1071/WF23175

© 2025 The Author(s) (or their employer(s)). Published by CSIRO Publishing on behalf of IAWF.

This is an open access article distributed under the Creative Commons Attribution-NonCommercial-NoDerivatives 4.0 International License (CC BY-NC-ND)

**OPEN ACCESS** 

#### **ABSTRACT**

Background. Current observational or instrumental records of past fires are historically limited, and information on fire characteristics tends to be confined to the recent past. Aims and methods. Here, we reconstruct a record of high-intensity fire events that extends beyond the historical record using carbon (C) and nitrogen (N) content and Fourier Transform Infrared (FTIR) spectroscopy applied to swamp sediment deposits in the Blue Mountains of south-eastern Australia. Each site has a different fire history over the past 50 years, and the known fire record was used to corroborate fire signatures before extending the record. Key results. FTIR spectra show an increase in the aromatic/aliphatic ratio for sediments corresponding to known fire events. Higher aromatic/aliphatic ratios suggest exposure to higher-intensity fire conditions. Conversely, the C and N content and C/N ratio show no association with known historic fire events. Conclusions. Sediment deposition at one site recorded three major fire events during the past ~500 years. Sediments recording the most recent fire event show a more significant increase in the aromatic/aliphatic ratio, suggesting that this event burnt at a higher intensity than the previous two. Implications. All sites show a promising extension of the existing fire record by decades to centuries.

**Keywords:** bushfires, carbon, fire history, fire intensity, FTIR spectroscopy, nitrogen, Southeastern Australia, swamp sediments.

#### Introduction

The Australian landscape is particularly susceptible to large bushfires, or wildfires, due to a combination of hot, dry weather conditions and volatile compounds in native vegetation species (Leigh *et al.* 2015). As climate change continues to alter the fire regime, it is expected that extreme fire weather and megafires will become more prominent in the landscape; however, the magnitude of this change remains a point of contention (Keeley and Syphard 2016). Retrospective measurements of fire characteristics, such as severity and intensity, can improve the predictive capabilities of models of future events (Whight and Bradstock 1999). Fire severity is characterised based on canopy consumption and ranges from low where the flames are confined to the understorey, to extreme where the canopy is completely consumed (Hammill and Bradstock 2006). Conversely, fire intensity is defined as the energy released by the fire front (Byram 1959).

Existing records of past fire and its characteristics currently span short periods of 30–60 years, particularly high-quality instrumental records (e.g. satellite data) (Chuvieco and Congalton 1989; Nedkov *et al.* 2018). Whilst tree rings can document the relationship between fire and climatic conditions, they remain challenging in the context of southeastern Australia. This is due to the lack of old-growth species outside of Tasmania, and many native species do not put down annual rings (Heinrich and Banks 2005). Analysis of charcoal accumulation and characteristics has long been used as a proxy for reconstructing past fire events due to its resistance to decomposition, allowing its preservation over long

timescales (Clark 1988; Blarquez *et al.* 2013). However, charcoal is highly susceptible to aeolian transportation through the convective processes associated with fire and could represent fires from outside of the catchment area. Without accurate, long-term (>100 years) records of past fire events and their characteristics, benchmarks cannot be established, and fire management practices remain limited in their capabilities (Williams *et al.* 2009).

Previous studies have used C and N content and the C/N ratio as proxies for past fire occurrence in sediment archives (e.g. Fernández et al. 1997; Krull et al. 2004; Santín et al. 2008; Silva-Sánchez et al. 2016). The C/N ratio typically decreases with increasing depth from the surface as a function of decomposition (Baldock and Skjemstad 2000). The relationship between the C/N ratio and fire is complex, with some studies finding an increase in the C/N ratio, suggested to arise from increased mobilisation of N to sediment deposits and reduced microbial respiration in sediments composed of fire products (Schmidt and Noack 2000; Krull et al. 2004; Barr et al. 2017), while others have identified a decreased C/N ratio, perhaps related to immobilisation of N or decreased organic matter content (Santín et al. 2008; Kaal et al. 2014; Abakumov et al. 2018). A severity dependence or no response has also been demonstrated (Martín et al. 2012; Araya et al. 2017). The C/N ratio is also highly influenced by vegetation (Forbes et al. 2021), which can be altered during a fire event. In contrast, C content has shown promising but varied results within fire-affected sediments. Fires typically result in an initial loss of C stores to the atmosphere through volatilisation as CO<sub>2</sub> or soot through the convective processes associated with the fire. However, a fraction of the biomass is converted to charcoal through a number of processes including pyrolysis, charring, charcoalification, and eventually forms ash (Conedera et al. 2009). This creates a continuum of products sometimes referred to as 'pyrogenic organic matter' or 'black carbon' (Conedera et al. 2009; Belcher et al. 2018), which may be highly recalcitrant due to the aromaticity of its chemical structure (Alexis et al. 2007; Kolka et al. 2014; Santín et al. 2016; Constantine et al. 2023). Additionally, net primary production increases during postfire regeneration, increasing carbon sequestration (Kuhry and Vitt 1996; van der Werf et al. 2017). Some studies have shown that reduced C content post-fire could take up to 2 years to recover to pre-fire stores (Martín et al. 2012). Other studies have reported no change in C content following a fire (Nave et al. 2011). This can result from the replenishment of C stores through litter-fall post-fire.

Fourier Transform Infrared (FTIR) spectroscopy of bulk sediments lends itself as a suitable proxy for extending fire records. Fires create a significant disturbance to peat swamps through increased temperature and pH, changed oxygen availability during combustion and the input of various combustion residues, significantly altering the chemical composition of the soil (Zaccone *et al.* 2014; Lupascu *et al.* 2020), which can be observed in the FTIR spectra. Organic

compounds are typically more vulnerable to transformation during a fire event, while mineral bonds require moderate to severe fires with higher temperatures (Zanelli *et al.* 2006; Araya *et al.* 2017). Aliphatic compounds are the first to be thermally decomposed during a fire event (Abakumov *et al.* 2018). These are replaced by aromatic compounds, which are more resistant to temperature and decomposition (Abakumov *et al.* 2018). Fire characteristics such as the temperature at ground level and the type of combustion (flaming or smouldering) can be inferred from the types of bonds present.

During a bushfire, the surface temperature of fine fuel loads can increase rapidly, and available oxygen for dispersion can be limited, forcing reactions to occur under a nitrogen atmosphere (Fang et al. 2006). This results in the removal of oxygen-containing functional groups and the conversion of amide-N into heterocyclic-N compounds (Almendros et al. 2003; Knicker et al. 2005). The heat of a fire typically does not infiltrate more than the top 5 cm of soil (Bradstock et al. 1992); therefore, the temperature of the fire at ground level can be estimated using the decomposition of various plant compounds such as cellulose, hemicellulose and lignin (Yang et al. 2007; Dorez et al. 2014).

Existing studies have used FTIR spectroscopy to explore changes in soil (e.g. Simkovic *et al.* 2008; Mastrolonardo *et al.* 2015*b*; Araya *et al.* 2017; Lu *et al.* 2022) and charcoal (e.g. Gosling *et al.* 2019; Constantine *et al.* 2021; Maezumi *et al.* 2021) following a fire event. Analysis of the peak area ratio of aromatic/aliphatic peak absorbance has also been shown to create a signature in alluvial sediment deposits following high-severity fires (Ryan *et al.* 2023), but the timescale at which this signature can be observed and the resolution at which individual fire events can be identified have not yet been explored.

This study aimed to produce a record of past fire events in mire sediment deposits using C and N content, the C/N ratio, and FTIR spectroscopy. Fire history was determined using remote sensing data, which outlines the burnt area of fires from 1957 to 2020 (Hammill *et al.* 2013; National Parks and Wildlife Service unpubl. data). Recent known fires (1993–2020) are accompanied by fire severity data (Hammill *et al.* 2013). Sediment samples were collected from Temperate Highland Peat Swamps on Sandstone (THPSS) in the Greater Blue Mountains World Heritage Area of New South Wales (NSW), Australia, a known fire hotspot. Well-dated sediment cores from mires can act as a suitable archive for past fire events due to their sensitivity to changes in regional climate, vegetation and nutrient supply (Dodson 1987).

### Materials and methods

### Study area

The Blue Mountains are located 50–100 km west of Sydney in New South Wales (NSW), Australia, accounting for

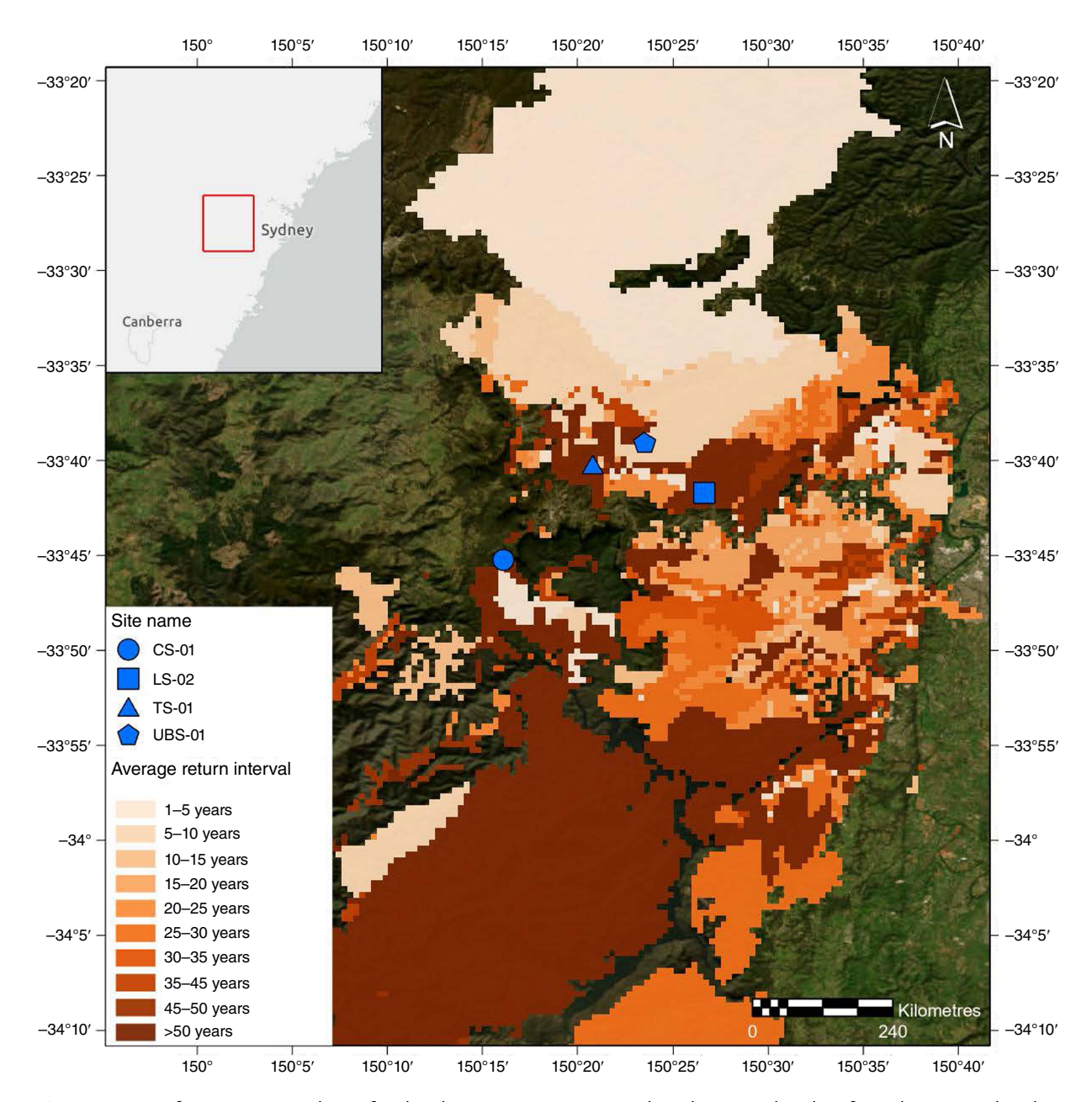


Fig. 1. Average fire return interval map for the Blue Mountains, New South Wales, Australia, identifying the sites analysed as Corral Swamp (CS-01, blue circle), Long Swamp (LS-02, blue square), Timmy's Swamp (TS-01, blue triangle), and Urella Brook Swamp (UBS-01, blue pentagon). Unshaded areas have not been burnt during the period from 1957 to 2020. Data adapted from NPWS (unpubl. data) and State Government of NSW and Department of Planning and Environment 2010. Satellite Image derived from: Esri, Maxar, GeoEye, Earthstar Geographics, CNES/Airbus DS, USDA, USGS, AeroGRID, IGN, and the GIS User Community Esri, HERE, Garmin, OpenStreetMap contributors, and the GIS User Community.

approximately 25% of the Greater Blue Mountains World Heritage Area (Fig. 1) (Cunningham 1984; Chapple *et al.* 2011; Tasker and Hammill 2011). The underlying geology is predominantly composed of sandstones with some shale lenses (Cunningham 1984; Dragovich and Morris 2002). Temperate Highland Peat Swamps on Sandstone (THPSS), or upland swamps, are a unique feature of the Blue Mountains and are typically situated at the headwaters of

low-order streams (Chalson and Martin 2009; Cowley et al. 2016; Fryirs et al. 2021). These upland swamps are generally low-energy environments but are highly erodible in the event of a disturbance, such as a bushfire (Chalson and Martin 2009; Fryirs et al. 2021). Dry sclerophyll forests dominated by *Eucalyptus* species are prevalent throughout much of the Blue Mountains; these vegetation communities are both fire-prone and fire-promoting due to the volatility

**Table 1.** Fire histories of the four study sites adapted from Hammill *et al.* (2013) and National Parks and Wildlife Services (NPWS) (unpubl. data).

Site	Fire season and type
Corral Swamp (CS-01) 33.7539°S, 150.2685°E	2019–2020, wildfire
Long Swamp (LS-02) 33.6951°S, 150.4439°E	1977–1978, wildfire 1982–1983, wildfire 1993–1994, wildfire 2002–2003, wildfire
Timmy's Swamp (TS-01) 33.6690°S, 150.3468°E	1957–1958, wildfire 1982–1983, wildfire 1993–1994, wildfire 2002–2003, wildfire 2019–2020, wildfire
Urella Brook Swamp (UBS-01) 33.6503°S, 150.3920°E	1982–1983, wildfire 1993–1994, wildfire 2002–2003, wildfire 2015–2016, prescribed burn 2019–2020, wildfire

Geodetic datum: WGS84.

of the oils within their leaves, increasing the susceptibility of the area to bushfires (Cunningham 1984; Bradstock et al. 2010; Aryal et al. 2018). The fire regime of the Blue Mountains traditionally consisted of frequent, low-intensity fires in the form of cultural burning by Aboriginal communities, or ignition from lightning strikes (Cunningham 1984). However, since British colonisation, this has shifted to high-intensity fire events with occasional prescribed burns (Dragovich and Morris 2002; Black et al. 2006). The topography of the Blue Mountains reduces accessibility to bushland and restricts control efforts of major bushfire events (Cunningham 1984), increasing the importance of more accurate predictive models for fire management.

This study analyses sediments collected from four upland swamps in the Upper Blue Mountains: (1) Corral Swamp (CS-01); (2) Long Swamp (LS-02); (3) Timmy's Swamp (TS-01); and (4) Urella Brook Swamp (UBS-01) (Fig. 1). Each site has experienced a different recent fire history and fire return interval (Table 1), and were selected to determine how fire characteristics have changed from 1957 to 2020. Fire history was determined using remote sensing data and digitised fire line maps (Hammill *et al.* 2013; National Parks and Wildlife Service, unpubl. data).

### Sample collection

In the field, sampling sites were selected to avoid creek lines and channels, which ensured that a more continuous record was collected. While the surface of the swamps is largely treeless, dominated by heath vegetation, the dry sclerophyll forest on the hillslope is likely the predominant source of bushfire-derived sediment. Based on this, the distance from the sampling site to the tree line was also determined. An approximately 25 cm deep monolith was collected at each site. Half of the bulk monolith was subsampled at 1-cm intervals for analysis.

## Elemental analysis

Elemental analysis of carbon (C) and nitrogen (N) was conducted at the Wollongong Isotope Geochronology Laboratory (WIGL) using an Elementar Vario Macro Cube Element Analyser. A total of 50 mg of each sample was ground to a fine, even powder for analysis. Three phenylalanine standards of different masses were analysed at the start of the sequence to formulate a calibration curve. Two blanks were also analysed prior to the phenylalanine standards and one blank before the samples. A repeat was analysed every four samples (n = 14), and a phenylalanine standard every 10–15 samples to account for drift. Carbon and N concentrations are reported in weight percent (wt%).

# Potassium bromide pressed disc (KBr) – FTIR spectroscopy

All samples were analysed for FTIR spectroscopy by KBr pressed discs at Comenius University using a Nicolet 6700 FTIR spectrometer and OMNIC 8 software (Thermo Fisher Scientific). Approximately 1 g of the bulk sediment of each sample was ground to a fine, homogeneous powder using a zirconium oxide mill and then dried at 60°C for 24 h. A total of 2 mg of each sample was combined with 200 mg of KBr and pressed into a pellet. Measurements were conducted in transmission mode across the 4000-400 cm<sup>-1</sup> range. Spectral bands form at specific wavenumbers when exposed to infrared light that can be reliably attributed to particular functional groups (Smidt et al. 2005; Beć et al. 2020). A total of 128 scans were averaged for each sample at a resolution of 2 cm<sup>-1</sup>, and the results were reported in absorbance values. The averaged spectra were baseline corrected in Python 3.8 using the 'arPLS' method (Baek et al. 2015) in the 'RamPy' package (Le Losq 2018). The baseline-corrected spectra were analysed for changes in peak height and peak area ratios, determined by taking the area under the curve for the bands of interest. A peak was considered as a ratio value >10, which is more than two standard deviations (s.d.) from the mean.

# Age-depth model determination

Three charcoal samples were selected from the top, middle, and bottom of the LS-02, TS-01 and UBS-01 sites for radiocarbon dating, with additional samples collected for the CS-01 site over a 100-cm D-section core. In addition, plant macrofossils, typically seeds isolated during wet sieving, were dated for CS-01 (12–13 and 23–24 cm), LS-02 (2–3) and 10-11 cm), TS-01 (10-11 cm), and UBS-01 (2-3 cm). Accelerator Mass Spectrometry (AMS) was performed at the Chronos <sup>14</sup>Carbon-Cycle facility, University of New South Wales (UNSW). Charcoal samples were prepared using an acid-base-acid treatment at 80°C with 1 M HCl and 0.2 M NaOH, as described by Turney et al. (2021). No pretreatment was applied to the seed samples due to their small size and fragility; therefore, each sample was rinsed with Milli-Q water and graphitised for analysis. Due to the absence of a chemical pre-treatment, the ages for these seed samples likely represent a minimum age. A Bayesian model employing Markov Chain Monte Carlo (MCMC) simulations was then formulated using OxCal ver. 4.4 with the P sequence deposition model and charcoal outlier model (Bronk Ramsey 2009). The charcoal outlier model was also applied to seed ages to account for their minimum age. The combine function was used when a seed and charcoal date were determined for the same depth (Bronk Ramsey 2009). The year of sampling at 0 cm was input into the model as an additional upper constraint. The 'SHCal 20' and 'Bomb 21 SH12' calibration curves were used to generate a calendar age-depth model (Hogg et al. 2020; Hua et al. 2021).

# **Results**

# Radiocarbon age-depth models

Seven radiocarbon ages between 0 and 100 cm were used in the final age-depth model for CS-01 (see Supplementary Table S1), giving a sedimentation rate that is in line with that observed in swamps in the Blue Mountains previously (e.g. Fryirs et al. 2014; Freidman and Fryirs 2015). The known fire history for this site identifies only the 2019-2020 bushfires. The LS-02 site uses a calendar year determined by individually calibrating the 2-3 cm seed date (Fig. S1b). Two ages were used in the final model for TS-01 (Table S1), and these ages are constrained by the bomb peak (Fig. S1c). Finally, four radiocarbon ages were determined for the UBS-01 site, with the combine function applied to the 2-3 cm charcoal and seed ages. The UBS-01 site has the oldest ages at the base of the monolith compared to any of the other sites and therefore has the slowest sedimentation rate. The age uncertainties for each sampling interval at this site are also the largest (Fig. S2g, h). For further details on the age-depth models see the Supplementary material.

#### Corral swamp

In the top 25 cm of the CS-01 sediment profile, the C content decreases slightly with increasing depth, ranging from 6.6 wt% (14–15 cm) to 25.8 wt% (4–5 cm). There are no obvious peaks (Fig. 2c). Nitrogen content shows no apparent trend with increasing depth and is consistently low, ranging

from 0.55 (14–15 cm) to 1.1 wt% (4–5 cm). No clear peaks are present in N content (Fig. 2*d*). The C/N ratio shows a general decreasing trend with increasing depth. Peaks are evident at 0–1 and 2–3 cm, and the C/N ratio ranges from 11.9 (14–15 cm) to 33.3 (2–3 cm) (Fig. 2*e*).

Various bands within the FTIR spectra highlight changes with depth. The CS-01 site shows the highest kaolinite O-H stretching absorbance at 3620-3695 cm<sup>-1</sup> (Zanelli et al. 2006; Yusiharni and Gilkes 2012) than any of the other sites (Fig. 2f). This is with the exception of the sample at 0-1 cm, where the absorbance is at baseline. Peak absorption in the bands associated with inorganic bonds at 600-950 cm<sup>-1</sup> (metal O-H bending) (Schroeder 2002) is lower than for the other sites. The quartz doublet at 797 and 779 cm<sup>-1</sup> (Dlapa et al. 2013; Aldeias et al. 2016) shows slight variation between samples and relatively low absorbance. All samples show high peak absorption in the band at 1200-1000 cm<sup>-1</sup>, which can be ascribed to both Si-O stretching of silicates, including clays, or C-O stretching predominantly from polysaccharides (Schroeder 2002; Krull et al. 2004; Nguyen et al. 2008; Hong et al. 2019) and absorbance is highly variable between samples. Generally, samples in the CS-01 site have the highest absorbance in the band associated with lignin products at ~1440 cm<sup>-1</sup> (aromatic C=C stretching, C-H bending of methyl and methylene groups) and 1375 cm<sup>-1</sup> (O-H bending of phenols, C-H bending of methyl group) (Artz et al. 2008; Keiluweit et al. 2010) than any of the other sites. Only the sample at 0-1 cm is at baseline, and the 14-15 cm sample shows a small reduction in peak height compared with the remaining samples. A small variation between samples is apparent in the broad band of aromatic C=C stretching at 1750-1500 cm<sup>-1</sup> accompanied by a shoulder at 1715-1740 cm<sup>-1</sup> due to C=O stretching of carbonyl groups in carboxylic acids, aldehydes, ketones, and esters (Mecozzi and Pietrantonio 2006). At 0-1 cm, aromatic C=C absorbance is higher than the remaining samples in this band. Aliphatic C-H stretching absorbance band at 3000-2800 cm<sup>-1</sup> (Dlapa et al. 2013; Mastrolonardo et al. 2015a; Cortizas et al. 2021) is also comparable between samples. The aromatic/aliphatic  $(A_{(1750-1500 \text{ cm}^{-1})}/(A_{(3000-2800 \text{ cm}^{-1})})$ ratio displays peaks at 0-1 cm and 14-15 cm depth (Fig. 2a). Conversely, the aromatic/inorganic ( $A_{(1750-1500)}$  $_{\text{cm}^{-1}}$ / $A_{(750-600 \text{ cm}^{-1})}$ ) peak area ratio shows peaks at 0-1 and 12-13 cm depth (Fig. 2b).

# Long Swamp

Carbon content of the LS-02 profile ranges from 10.8 wt% (18–19 cm) to 39.4 wt% (10–11 cm). The C content shows minimal variation until  $\sim$ 14–15 cm depth, where there is a decrease (Fig. 3c). Nitrogen content ranges from 0.45 wt% (18–19 cm) to 1.7 wt% (12–13 cm). Nitrogen content shows minimal variation above 14–15 cm, below which there is a decrease, with negative excursions evident at 14–15 and

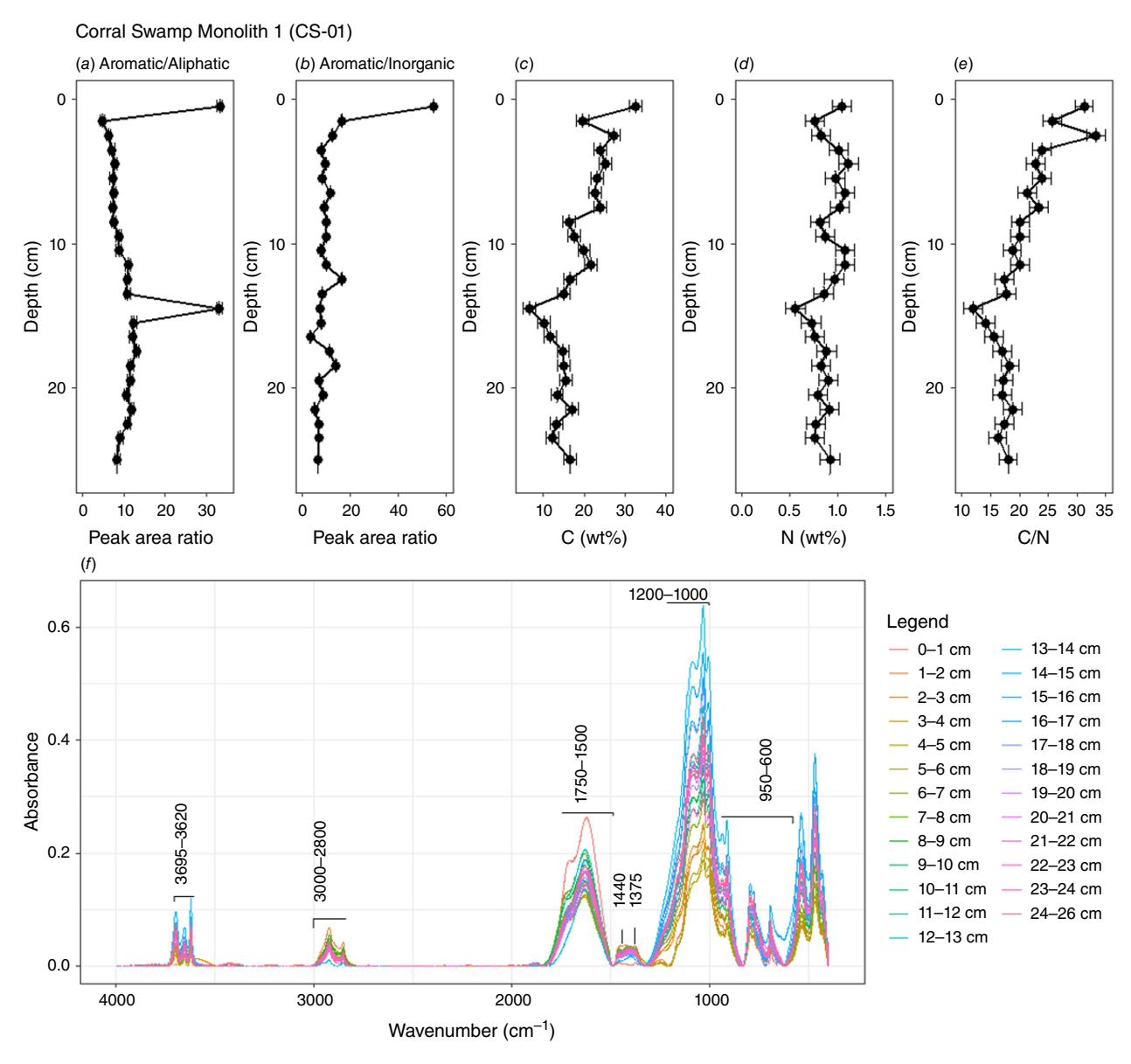


Fig. 2. Peak area ratios for (a) aromatic/aliphatic ( $A_{(1750-1500 \text{ cm}^{-1})}$ /( $A_{(3000-2800 \text{ cm}^{-1})}$ ) and (b) aromatic/inorganic ( $A_{(1750-1500 \text{ cm}^{-1})}$ /  $A_{(750-600 \text{ cm}^{-1})}$ ) peak intensities with relation to depth. (c) and (d) are the C and N content, respectively (reported in wt%), and (e) the C/N ratio (unitless). (f) The complete FTIR spectra from 4000 to 400 cm<sup>-1</sup> for the CS-01 site. Labelled ranges denote key bands referenced in the text.

18–19 cm depth (Fig. 3*d*). The C/N ratio displays no obvious trends with depth and varies over a range of 17.2 (19–20 cm) to 28.5 (7–8 cm). Peaks are evident at 4–5, 7–8 and 18–19 cm depth (Fig. 3e).

The LS-02 profile shows a high variability between samples in the bands associated with organic and inorganic bonds (Fig. 3f). Low peak absorbance is evident across all samples in the band at 3620–3695 cm<sup>-1</sup> associated with O–H stretching of kaolinite. Samples at 14–21 cm have a higher absorbance in the bands at 600–950 cm<sup>-1</sup> (associated with metal O–H bending) and within the quartz doublet at 797 and 779 cm<sup>-1</sup>. These samples show much lower peak

height in bands associated with aromatic C=C absorbance at 1750–1500 cm<sup>-1</sup>, aliphatic C–H stretching at 3000–2800 cm<sup>-1</sup>, and lignin products. Conversely, samples at 0–13 cm show a lower peak height for inorganic bonds and for the quartz doublet (797 and 779 cm<sup>-1</sup>). However, absorbance associated with aromatic C=C absorbance at 1750–1500 cm<sup>-1</sup>, aliphatic C–H stretching at 3000–2800 cm<sup>-1</sup>, and bands ascribed to lignin products at 1440 and 1375 cm<sup>-1</sup> are higher for these depths. Aliphatic C–H stretching shows the highest peak height of any other site. All samples display varying peak shapes and heights in the band from 1200 to 1000 cm<sup>-1</sup>, ascribed to both Si–O bonds of clay and C–O

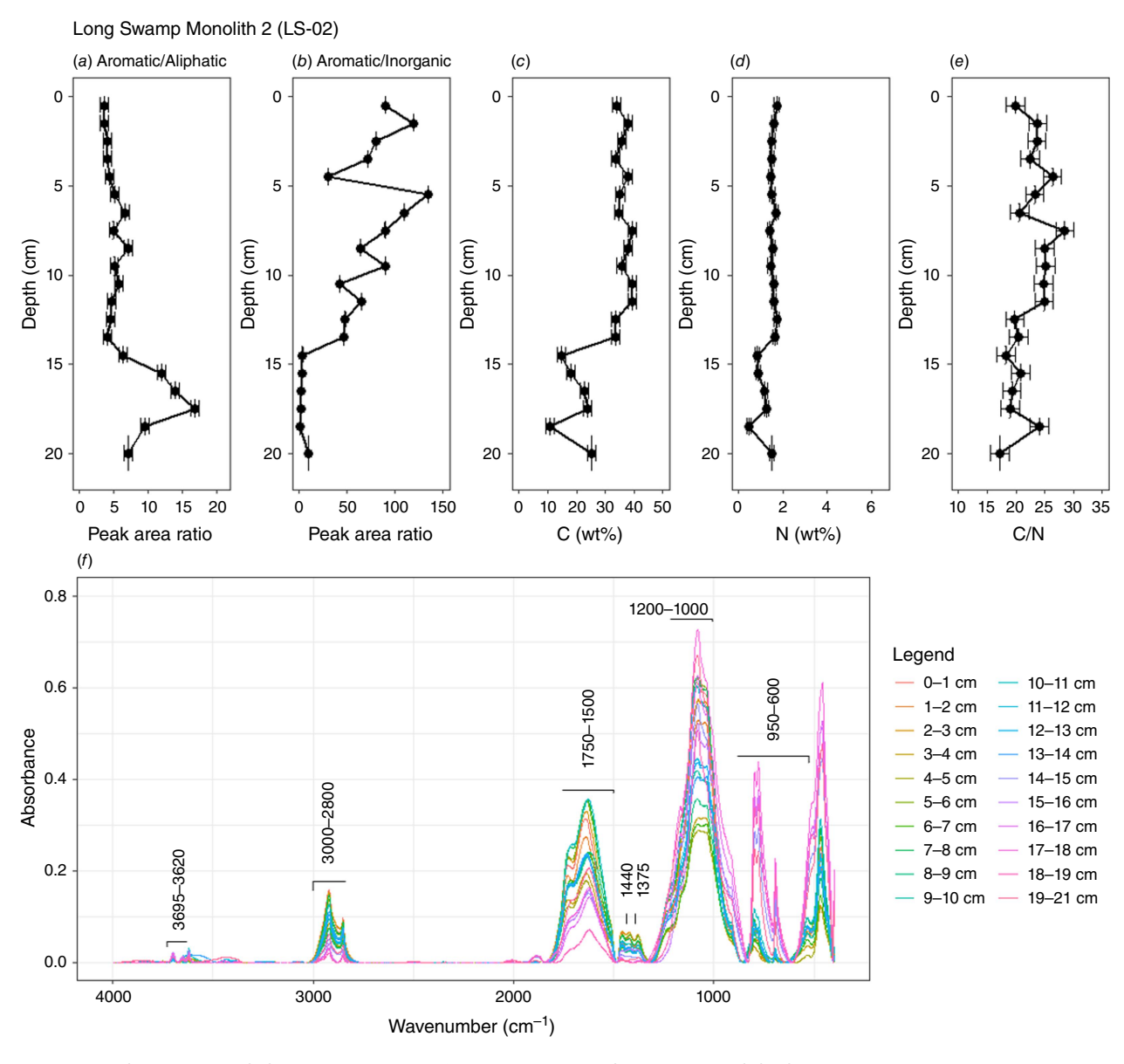


Fig. 3. (a) The aromatic/aliphatic  $(A_{(1750-1500 \text{ cm}^{-1})}/(A_{(3000-2800 \text{ cm}^{-1})})$  peak area ratio and (b) the aromatic/inorganic  $(A_{(1750-1500 \text{ cm}^{-1})}/A_{(750-600 \text{ cm}^{-1})})$  ratio, (c) and (d) are the C and N content, respectively (reported in wt%), and (e) the C/N ratio (unitless). (f) The complete spectra from 4000 to 400 cm<sup>-1</sup> for the LS-02 site. Labelled ranges denote key bands referenced in the text.

bonds of polysaccharides. The aromatic/aliphatic ratio shows only one prominent peak at 17–18 cm (Fig. 3a). The aromatic/inorganic ratio, however, displays peaks at 1–2, 5–6, 9–10 and 11–12 cm (Fig. 3b)

# Timmy's Swamp

The C content ranges from 2.8 wt% (11–12 cm) to 17 wt% (0–1 cm), displaying a general decreasing trend with increasing depth. Peaks are apparent at 0–1 and 3–4 cm depth (Fig. 4c). N content shows minimal variation between samples, ranging from 0.15 wt% (13–14 cm) to 0.55 wt% (0–1 cm) and a decreasing trend with increasing depth.

(Fig. 4*d*). The C/N ratio decreases slightly with increasing depth, with values ranging from 13.9 (18–19 cm) to 29.9 cm (0–1 cm). Possible peaks are observed at 0–1, 2–4, 8–9, and 13–14 cm (Fig. 4e).

Various organic and inorganic bands show changes in peak height with depth at the TS-01 site (Fig. 4*f*). All samples show minimal absorption at 3620–3695 cm<sup>-1</sup>. Inorganic bonds in the bands from 600 to 950 cm<sup>-1</sup> (metal O–H bending) and from 700 to 1200 cm<sup>-1</sup> (Si–O and Al–O stretching) show high peak absorption for most samples; however, it is highly variable. The quartz doublet at 797 and 779 cm<sup>-1</sup> varies between samples but is particularly high between 3–4 and 18–22 cm. The peak shape and

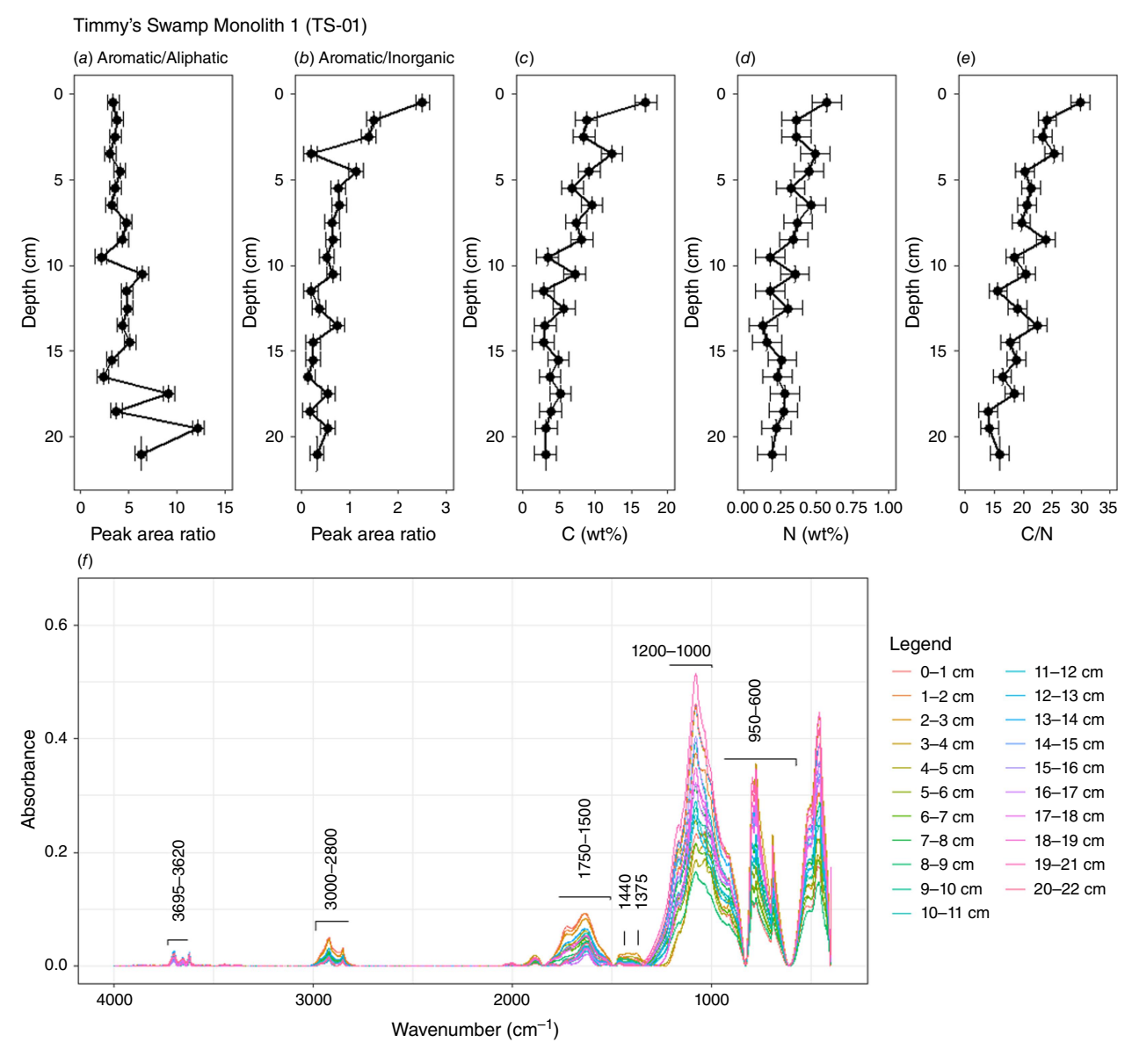


Fig. 4. Peak area ratios for (a) aromatic/aliphatic ( $A_{(1750-1500 \text{ cm}^{-1})}$ /( $A_{(3000-2800 \text{ cm}^{-1})}$ ) and (b) aromatic/inorganic ( $A_{(1750-1500 \text{ cm}^{-1})}$ /  $A_{(750-600 \text{ cm}^{-1})}$ ) peak intensities with relation to depth, (c) and (d) are the C and N content, respectively (reported in wt%), and (e) the C/N ratio (unitless). (f) The complete FTIR spectra from 4000 to 400 cm<sup>-1</sup> for the TS-01 site. Labelled ranges denote key bands referenced in the text.

height in the band between 1200 and 1000 cm<sup>-1</sup> (C–O groups of polysaccharides and Si–O bonds of clays) varies between samples. Few depths show higher than background in the band at ~1440 and 1375 cm<sup>-1</sup>, associated with the lignin products. The top 3 cm have the highest absorbance in the band at 3000–2800 cm<sup>-1</sup> associated with aliphatic C–H stretching bonds, but all samples have low peak heights within this band, suggesting lower organic matter content. Aromatic C=C absorbance at 1750–1500 cm<sup>-1</sup> is also low compared with the other sites analysed. The aromatic/aliphatic peak area ratio shows a general decreasing trend with increasing depth and only two peaks at 17–18 and 19–20 cm (Fig. 4a). The aromatic/inorganic peak area ratio shows a

general decreasing trend with increasing depth. Whilst the peak area is highest at the surface, this does not constitute a peak compared to the other sites analysed (Fig. 4b).

# **Urella Brook Swamp**

The C content ranges from 5.85 wt% (14–15 cm) to 40.65 wt% (1–2 cm), following a general decreasing trend with increasing depth. Peaks are evident at 1–2, 8–9 and 19–20 cm (Fig. 5c). The N content has a much smaller range over much of the profile, ranging from 0.4 wt% (12–13 cm) to 1.25 wt% (2–3 cm) (Fig. 5d). The C/N ratio ranges from 14.6 (16–17 cm) to 35.5 (1–2 cm) and

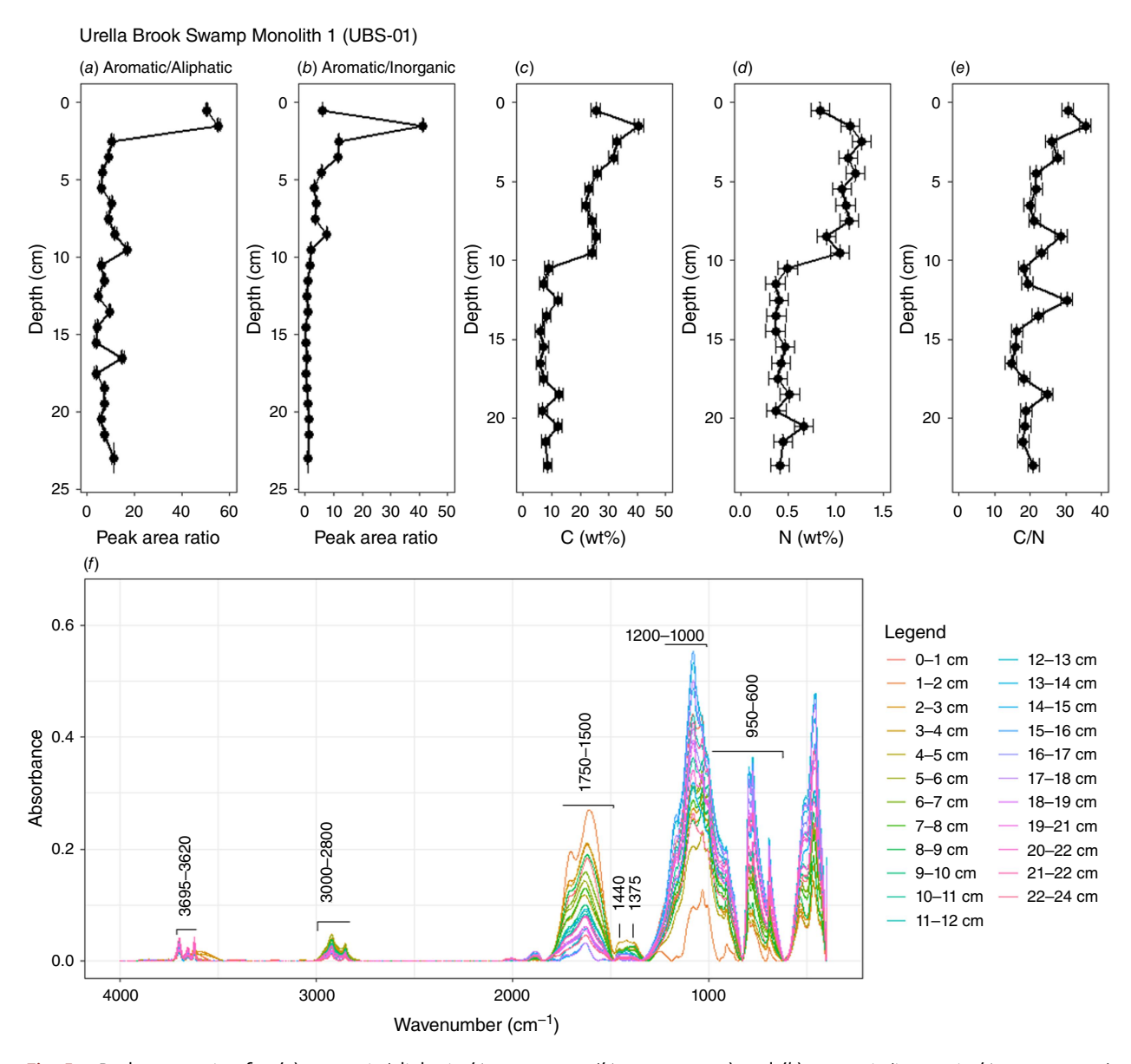


Fig. 5. Peak area ratios for (a) aromatic/aliphatic  $(A_{(1750-1500 \text{ cm}^{-1})}/(A_{(3000-2800 \text{ cm}^{-1})})$  and (b) aromatic/inorganic  $(A_{(1750-1500 \text{ cm}^{-1})}/A_{(750-600 \text{ cm}^{-1})})$  peak intensities with relation to depth, (c) and (d) are the C and N content (reported in wt%), respectively, and (e) the C/N ratio (unitless). (f) The complete FTIR spectra from 4000 to 400 cm<sup>-1</sup> for the UBS-01 site.

is relatively constant with depth, highlighting peaks at 1–2, 3–4, 8–9, 12–13, and 18–19 cm (Fig. 5*e*).

Bands associated with organic and inorganic bonds show changes in peak height across the spectra for each sample (Fig. 5*f*). All samples show low peak height at 3620–3695 cm<sup>-1</sup> associated with O–H stretching of kaolinite. The top 10 cm have the lowest peak absorbance at the doublet at 797 and 779 cm<sup>-1</sup> associated with quartz. The band at 1200–1000 cm<sup>-1</sup> shows a range of peak heights and shapes. The 1–2 cm depth sample has the lowest peak height within this region. Peak absorption in the region from 600 to 950 cm<sup>-1</sup>, highlights large variation between samples. At 1–2

cm, absorption is particularly low. The band at 700–1200 cm $^{-1}$  also shows large variation between samples. The bands at  $\sim$ 1440 cm $^{-1}$  and 1375 cm $^{-1}$  show an increase in absorbance for some samples, whilst others remain close to background. Aliphatic C–H stretching bonds at 3000–2800 cm $^{-1}$  are relatively low and comparable across all samples. Aromatic C=C bonds at 1750–1500 cm $^{-1}$  show a larger range, with 1–2 cm depth having the highest peak height and 14–15 cm depth with the lowest. The peak area ratio of aromatic/aliphatic shows peaks at 0–2, 9–10 and 16–17 cm (Fig. 5a), whilst the aromatic/inorganic ratio displays peaks at 1–2 and 8–9 cm (Fig. 5b).

#### Discussion

#### Sedimentation rate

The sedimentation rate over the four sites varies from 0.05 cm/year (Urella Brook Swamp) to 0.341 cm/year (Timmy's Swamp) (Fig. S2). Existing studies have also shown variable sedimentation rates for similar environments (Fryirs et al. 2014; Freidman and Fryirs 2015; Mooney et al. 2021). It has been hypothesised that this variation in sedimentation rate reflects catchment stability, whereby a slower sedimentation rate is associated with greater stability and faster sedimentation with instability (Fryirs et al. 2014). Vegetation cover, air temperature, rainfall, and fire frequency and intensity affect erosion rates and subsequent catchment stability (Fryirs et al. 2014; Mooney et al. 2021). Additionally, the sedimentation rate tends to decrease exponentially with increasing depth from the surface due to compression. Previous studies have typically dated samples below 20 cm depth; therefore, the ages determined across all four sites are relatively young, and although further comparison is challenging, these results demonstrate that over the past century, sediments have accumulated in THPSS at a rate varying between ~5 and 34 cm/100 years.

# Fire occurrence in the sediment record

Based on the radiocarbon-based chronology of the sediment deposits studied and assuming no lag between a fire event and its record in the sediment deposits, we expect fire events to be recorded at the depths in Table 2. After a fire event, organic and inorganic material is transported to the swamp, possibly during a post-fire rainfall event. This may create layers associated with the fire event represented by a change in the chemical composition compared to the sediments that have not been affected by fires.

# Carbon and nitrogen abundance

Despite previous studies suggesting an increase in N content in fire-affected sediments due to increased erosion of soils, combusted leaf litter and ash enriched in nutrients, including N post-fire (Thomas *et al.* 1999; Lane *et al.* 2008), there appears to be no significant increase in N content in layers hypothesised to record fires (Fig. S3b, *e*, *h*, *k*).

Whilst there is a small increase in C content for the uppermost fire layer in the CS-01 and UBS-01 sites, no significant correlation exists between C content and fire occurrence at the other sites (Fig. S3a, d, g, j). This agrees with the results reported by Alexis et al. (2007) and Martín et al. (2012), who found a similar, limited response to fire events. Fire in nutrient-limited landscapes, such as the Blue Mountains, is believed to release nutrients (Raison et al. 1985; Orians and Milewski 2007). Therefore, it is surprising that there is no consistent change in C content with fire.

**Table 2.** Expected depths of fire events based on the radiocarbon-based age—depth model at each site.

Site	Depth (cm)	Fire event
Corral Swamp (CS-01)	0.5	2019–2020, wildfire
Long Swamp (LS-02)	4	2002–2003, wildfire
	5	1993–1994, wildfire
	6.5	1982–1983, wildfire
	7.5	1977–1978, wildfire
Timmy's Swamp (TS-01)	0.5	2019–2020, wildfire
	3.5–4	2002–2003, wildfire
	7	1993–1994, wildfire
	11–11.5	1982–1983, wildfire
	20.5–21	1957–1958, wildfire
Urella Brook Swamp (UBS-01)	0	2019–2020, wildfire
	0.5	2015–2016, pescribed burn
	2.5	2002–2003, wildfire
	3	1993–1994, wildfire
	3.5–4	1982–1983, wildfire

The C/N ratio typically decreases within increasing depth due to increased decomposition (Krull *et al.* 2004); however, many studies have shown a variable response to fire (e.g. Fernández *et al.* 1997; Santín *et al.* 2008; Martín *et al.* 2012; Sazawa *et al.* 2018). In this study, there are no consistent trends with layers hypothesised to record known fire events and the C/N ratio for any of the four sites (Fig. S3c, f, i, l). For additional discussion of the C and N abundances, see the Supplementary material.

# FTIR spectra

Aliphatic C-H bonds occur at 2920 cm<sup>-1</sup> (asymmetric stretching vibrations) and 2860 cm<sup>-1</sup> (symmetric stretching vibrations). Previous studies have combined these two bands, allocating the range from 3000 to 2800 cm<sup>-1</sup> to aliphatic bonds (Guo and Bustin 1998; Ellerbrock et al. 2005; Lammers et al. 2009). Aliphatic bonds are typically attributed to fats, plant waxes, lignin, etc. (Guénon et al. 2013; Wu et al. 2020) and have been shown to decrease with depth due to increasing humification (Artz et al. 2008). Aliphatic compounds are the first to be decomposed at elevated temperatures during a fire event (Abakumov et al. 2018). Decomposition of aliphatic bonds typically occurs at temperatures > 250°C or with prolonged heating duration, resulting in a relative increase in aromatic peak contributions through Diels-Alder type reactions, which are more resistant to higher temperatures and decomposition (Guo and Bustin 1998; Rausa et al. 1999; Araya et al. 2017). The aromatic/aliphatic peak area ratio of sediment deposits could thus identify past events where organic compounds experienced higher intensity fire conditions, including higher temperatures and/or longer heating duration. There can be some contributions from O-H bending vibrations of water between phyllosilicate layers (Madejová 2003). However, there is a strong positive correlation between C content and the peak area of aromatic absorption, suggesting aromatic C is more dominant in this band (Fig. S4). Therefore, we assume that sediments with higher aromatic/aliphatic ratio values record past fire events. Bradstock et al (2010) and Collins 2014 have correlated fire severity with estimated fire fire intensity in the broader Sydney Basin with underlying sandstone geology, therefore, the high intensity fires recorded by the FTIR spectra are likely canopy consuming events. Applying the radiocarbonbased age-depth model to the CS-01 site identifies peaks in the aromatic/aliphatic ratio at the surface and at 14-15 cm (1887 (+66/-170) CE) (Fig. 6a). Both peaks show a similar value. The 2019-2020 bushfire is the only known fire recorded for this site and likely corresponds with the peak at the surface. The Blue Mountains experienced bushfires in 1888-1889, 1895-1896, 1904-1905, 1908-1909, 1911-1912, and 1915-1916 CE (Cunningham 1984) that are within the age-model error. Therefore, the deeper peak in the aromatic/aliphatic ratio could correspond to one of these events.

For the LS-02 site, there is one peak at 17-18 cm (1955) (+5/-2) CE), which is older than the extent of the known fire history for this site (Fig. 6b). The known fire history identifies four more recent fires in 1977-1978, 1982-1983, 1993-1994, and 2002-2003, which are not associated with aromatic/aliphatic ratios > 10 in the sediment deposit. Ryan et al. (2023) found that charcoal layers in sediments of small-order creek beds were ~700 years old at approximately 20 cm depth and hypothesised that the charcoal was being stored on the hillslope for many years before deposition. Therefore, it is possible that this peak represents a high-intensity fire in the 1950s, and fire products from more recent events have not yet been mobilised by rainfall from the hillslope to the swamp sequence vet. Since the the Blue Mountains have experienced Millennium drought (1997-2009), which recorded the lowest 13-year rainfall total in the instrumental record (Timbal and Fawcett 2013) and was followed by consecutive positive Indian Ocean Dipoles (IOD) and El Niño events in 2018 and 2019 (Wang and Cai 2020). If the sediments were stabilised by vegetation regrowth before a major rainfall event, this could have caused a lag between the fire and the fire-related sediments reaching the swamp deposit.

Only one peak was identified in the TS-01 profile corresponding with  $1960 \pm 7$  CE in the age–depth model (Fig. 6c). This peak is within error of the 1957–1958 fire. Similar to LS-02, this suggests that sediments corresponding to the 1982–1983, 1993–1994, 2002–2003, and 2019–2020 fires have not yet been deposited in the sediment record at this site. The UBS-01 site has the longest record of the four

sites and displays peaks in the aromatic/aliphatic ratio associated with dates of 2017 (+2/-10) CE, 2011 (+3/-31)CE, 1882 (+84/-101) CE and 1737 (+157/-121) CE from the model (Fig. 6d). Since this site has the longest record over similar depths to the remaining three sites, the resolution is coarser, and peaks are therefore attributed to major fire events. The peaks at 2017 (+2/-10) CE and 2011 (+3/-31) CE have ratios of  $\sim$ 50 and  $\sim$ 55, respectively, which are more than three times greater than the peaks at 1882 (+84/-101) CE and 1737 (+157/-121) CE. These increases in aromatic/aliphatic ratio, possibly associated with the 2017 (+2/-10) CE and 2011 (+3/-31) CE fires, suggest that their intensity could have been greater than the fires hypothesised to have occurred in the 18th and 19th centuries. The age range for this peak at 0-2 cm is between 1980 and 2019 CE. Owing to this uncertainty, it is not possible to confidently attribute this peak to a known fire event.

The aromatic/inorganic peak area ratio can provide information on the organic matter content of samples  $(A_{(1750-1500\text{cm}^{-1})}/A_{(750-600\text{cm}^{-1})})$ . The band at 750–600 cm<sup>-1</sup> is ascribed to Si-O bending vibrations (Farmer 1974; Hahn et al. 2018) and does not undergo dehydroxylation at the temperatures reached during a bushfire. Whilst the CS-01 site shows peaks of similar magnitude relating to the 2019–2020 and 1887 (+66/-170) CE fire events, this is not replicated in the aromatic/inorganic ratio (Fig. 6e), with only the peak at the surface correlating with the 2019-2020 fire present. Similarly, the peak at the surface of the UBS-01 site is prominent and in agreement with the aromatic/aliphatic ratio, whilst the second peak is slightly offset to 1907 (+47/-94) CE (1887 (+66/-170) CE for the aromatic/aliphatic ratio); however, this is still within the uncertainty of the age-depth model (Fig. 6h). Unlike the aromatic/aliphatic ratio, there are no peaks in the aromatic/ inorganic ratio at 14-15 cm depth. This suggests that inorganic material is more dominant in this sediment.

Unlike the other sites, the TS-01 site has a much lower aromatic/inorganic peak area ratio across all samples (Fig. 6g). The peak intensity for all organic bands in the TS-01 site is also lower than that of any other sites, indicating an overall lower organic matter content. The aromatic/inorganic peak area ratio is the highest at the surface and decreases with increasing depth, which is expected considering it is hypothesised to represent the organic matter content. Peat-dominated environments typically have a high water-holding capacity due to the low bulk density and high pore volume of organic matter (Huat et al. 2011). The TS-01 site has the lowest moisture content of the four sites, possibly explaining this reduction in organic matter content.

At the LS-02 site, the aromatic/inorganic ratio does not show peaks at the same depths as the aromatic/aliphatic ratio (Fig. 6b, f). Peaks are found at depths not ascribed to a known fire event, possibly due to the higher organic content

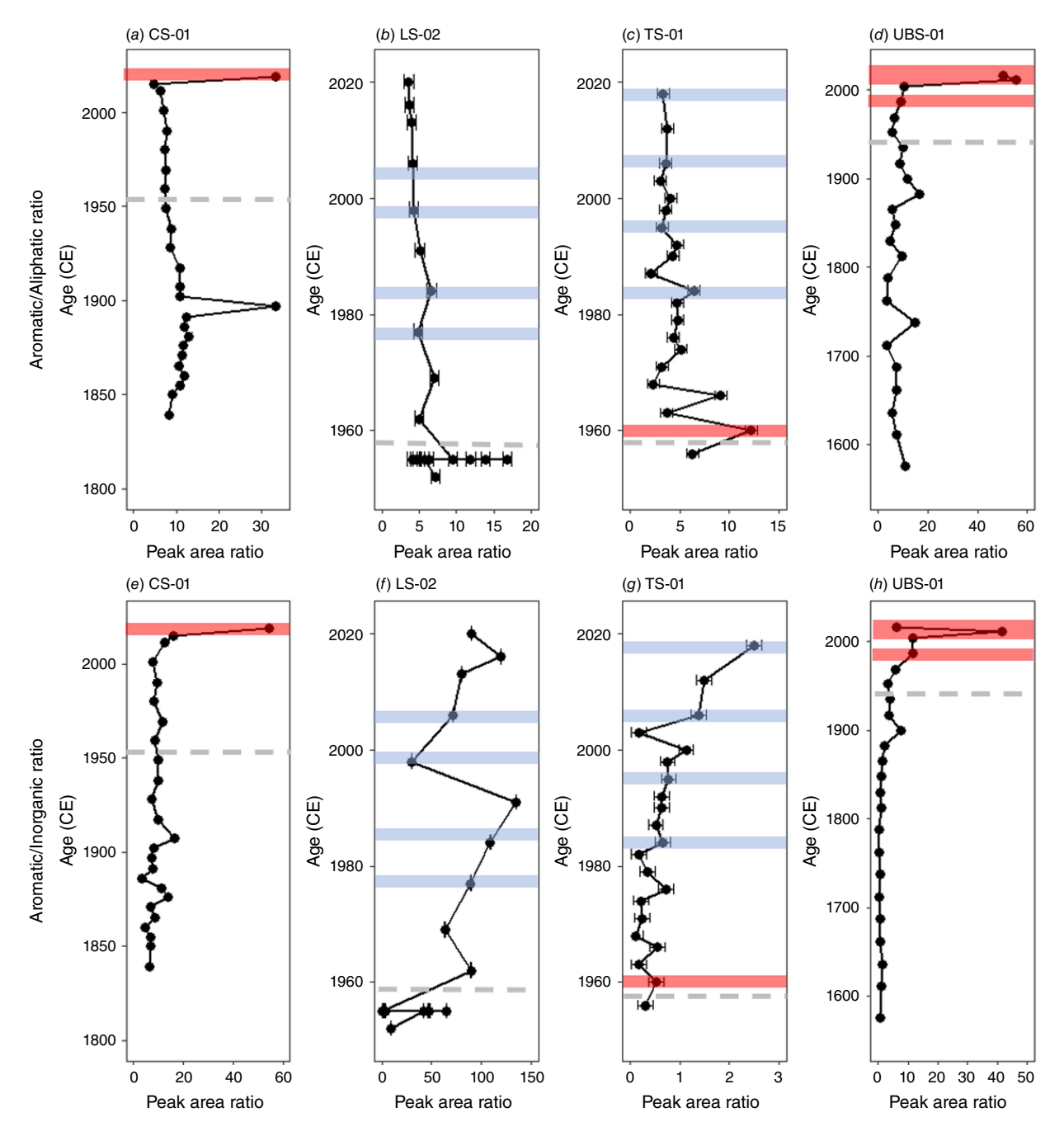


Fig. 6. (a-d) The aromatic/aliphatic ratio with relation to the age-depth model for CS-01, LS-02, TS-01 and UBS-01, respectively. (e-h) The aromatic/inorganic ratio for CS-01, LS-02, TS-01 and UBS-01, respectively. Red shading, known fire events correlated with peaks in the respective ratios; blue shading, other known fire events expected in the record. Where applicable, the grey dotted line indicates the extent of the known fire record. Age uncertainties are in Fig. S1b, d, f, h.

of the majority of this monolith. There is a greater than tenfold increase in inorganic peak intensity at 14–19 cm depth, meaning that any change in aromatic peak absorbance has little effect on the aromatic/inorganic ratio. This peak in inorganic intensity is also accompanied by an increase in the sedimentation rate (Fig. S1c). Catchment instability can cause a significant increase in the accumulation rate of swamps, specifically inorganic compounds

(Fryirs *et al.* 2014; Mooney *et al.* 2021). This instability can result from various disturbances, particularly fire and large-scale rainfall events (Fryirs *et al.* 2014; Mooney *et al.* 2021). Peaks in the aromatic/inorganic ratio are ascribed to 2016 (+4/-3) CE, 1984 (+7/-3) CE, and 1962 (+8/-2) CE. There is a significant decrease in the aromatic/inorganic ratio at 17–18 cm (1955 (+5/-2) CE), which was associated with a peak in the aromatic/aliphatic ratio. During this

period, the World War II drought (1939–45) (Freund *et al.* 2017) could have increased the instability of the catchment and the subsequent increase in inorganic materials in the sediment.

Kaolinite can be attributed to peaks at 3700-3600 cm<sup>-1</sup> assigned to O-H stretching vibrations (Berna et al. 2007; Yusiharni and Gilkes 2012; Cortizas et al. 2021). Samples from the TS-01, LS-02 and UBS-01 sites all have very low peak absorption in this band (Figs. 3f, 4f, 5f). Samples from CS-01 show a higher peak absorption (Fig. 2f); however, the sample at 0-1 cm, attributed to the 2019-2020 bushfire, displays no peak at 3700-3600 cm<sup>-1</sup>. One hypothesis for this is the transformation of kaolinite at high temperatures. Dehydroxylation weakens the O-H stretching band at 400°C and destroys it at 530°C (de Santana et al. 2006; Berna et al. 2007). Whilst the destruction of the structure of other clay minerals, such as smectite and illite, occurs gradually, the loss of structural water from kaolinite is more abrupt (Berna et al. 2007). This tends to form a broad band centred at ~3450 cm<sup>-1</sup>, typical of metakaolinite, suggesting that temperatures could have been greater than 530°C during this fire. There is no obvious decrease in peak height for identified fire layers at any other site. Alternatively, there may be a delay in kaolinite deposition at the surface of the profile. Organic matter may be lost by the volatilisation and convective processes of the fire, whilst inorganic matter is more commonly transported by channel erosion and increased runoff (Shakesby and Doerr 2006). However, this seems less likely given that major rainfall events occurred in short succession following the 2019-2020 bushfires, providing an opportunity for the erosion of kaolinite.

Clay content can also be reflected in the peaks at 1100–1000 cm<sup>-1</sup>. Si–O stretching vibrations create peaks in this range (Haberhauer *et al.* 1998; Krull *et al.* 2004). However, it is important to note that polysaccharides are also visible in this region, with C–O groups attributed to the band at 1036 cm<sup>-1</sup> (Haberhauer *et al.* 1998; Krull *et al.* 2004; Nguyen *et al.* 2008). This band represents a range of peak absorption between the four sites. Given that organic matter predominates within these swamps, absorption relating to polysaccharides is likely to contribute more to this band; however, Si–O absorption of clays cannot be ruled out.

The Si–O peaks attributed to quartz are absorbed across several bands. The most prominent is the doublet at 778 and 798 cm<sup>-1</sup> associated with SiO<sub>4</sub> symmetric stretching; however, Si–O–Si bending transitions are also absorbed at 698 cm<sup>-1</sup> and antisymmetric SiO<sub>4</sub> stretching to 1084 cm<sup>-1</sup> (Dlapa *et al.* 2013; Aldeias *et al.* 2016; Hahn *et al.* 2018). There is a large variation in quartz absorption across all sites. CS-01 has the lowest peak absorption across all samples. TS-01 and UBS-01 show no significant trend with depth. However, LS-02 highlights a significant increase in quartz absorption at 14–21 cm. This suggests a possible in-wash event, depositing coarser-grained material at these depths.

Peaks attributed to organic materials can also reflect the temperature and characteristics of the fire. The structural units of lignin may be responsible for the observed bands at 1440 cm<sup>-1</sup> (aromatic C=C stretching) and 1375 cm<sup>-1</sup> (O-H bending of phenols) (Keiluweit et al. 2010). Lignin begins to break down at temperatures of 160-300°C (Keiluweit et al. 2010; Dorez et al. 2014; Mastrolonardo et al. 2015b; El Atfy et al. 2017). Heating to these relatively low temperatures alters the distribution of phenols, but the majority of the structure will remain unaltered (Mastrolonardo et al. 2015b). Above 500°C, the degree of condensation is increased, and lignin is destroyed at around 900°C (Keiluweit et al. 2010; El Atfy et al. 2017). While the TS-01 and UBS-01 sites show no significant trend, the LS-02 site shows a lower peak height in the band ascribed to lignin for samples with higher inorganic absorption. CS-01 shows relatively similar peak height across all samples, except those affected by fire. There is a slight decrease in peak height associated with the 1887 (+66/-170) CE fire layer, but the sediments associated with the 2019-2020 fire show no absorption in this band at all, suggesting that the temperature of the 2019–20 fires could have been in excess of 900°C in the catchment area of the sediment core. Alternatively, this reduction in peak height may have resulted from a longer heating duration during the 2019-2020 bushfire. Longer heating durations increase the temperature of the surface soils and bark, allowing increased heat transfer compared to a faster-moving fire (Aldeias et al. 2016), thus resulting in a similar change observed in the FTIR spectra.

#### **Conclusions**

We aimed to assess how the C and N content, C/N ratio, and FTIR spectra of sediment deposits record past fire in the Upper Blue Mountains of New South Wales, Australia. All sites recovered sediments spanning the known fire history, and two sites (Corral Swamp and Urella Brook Swamp) extended several decades to centuries beyond. Peak area ratios of aromatic/aliphatic compounds were used as a proxy to identify sediments exposed to higher-intensity fire conditions. At least one high-intensity fire was identified in all four of the sites. The UBS-01 site showed a significant increase in the aromatic/aliphatic ratio at the surface compared with the two remaining fires identified at the site. An increased temperature or heating duration during the 2019-20 bushfire compared with the fire event dated to 1887 (+66/-170) CE was also shown by the elimination of the band ascribed to lignin at the CS-01 site. The C and N content and C/N ratio showed no consistent trend between sites, suggesting that these parameters are less effective at identifying fire events in this landscape. The resolution of the record was found to be a limitation at some sites, and some of the known fires had not yet been deposited within

the record, suggesting possible storage on the hillslope. While more data are needed to more confidently discern trends in past fire intensity, these results show a promising extension of the existing fire record.

# Supplementary material

Supplementary material is available online.

#### References

- Abakumov E, Maksimova E, Tsibart A (2018) Assessment of postfire soils degradation dynamics: stability and molecular composition of humic acids with use of spectroscopy methods. *Land Degradation and Development* **29**, 2092–2101. doi:10.1002/ldr.2872
- Aldeias V, Dibble HL, Sandgathe D, Goldberg P, McPherron SJP (2016) How heat alters underlying deposits and implications for archaeological fire features: a controlled experiment. *Journal of Archaeological Science* **67**, 64–79. doi:10.1016/j.jas.2016.01.016
- Alexis MA, Rasse DP, Rumpel C, Bardoux G, Péchot N, Schmalzer P, Drake B, Mariotti A (2007) Fire impact on C and N losses and charcoal production in a scrub oak ecosystem. *Biogeochemistry* **82**, 201–216. doi:10.1007/s10533-006-9063-1
- Almendros G, Knicker H, González-Vila FJ (2003) Rearrangement of carbon and nitrogen forms in peat after progressive thermal oxidation as determined by solid-state <sup>13</sup>C- and <sup>15</sup>N-NMR spectroscopy. *Organic Geochemistry* **34**, 1559–1568. doi:10.1016/S0146-6380(03)00152-9
- Araya SN, Fogel ML, Berhe AA (2017) Thermal alteration of soil organic matter properties: a systematic study to infer response of Sierra Nevada climosequence soils to forest fires. *Soil* **3**, 31–44. doi:10.5194/soil-3-31-2017
- Artz RRE, Chapman SJ, Jean Robertson AH, Potts JM, Laggoun-Défarge F, Gogo S, Comont L, Disnar JR, Francez AJ (2008) FTIR spectroscopy can be used as a screening tool for organic matter quality in regenerating cutover peatlands. *Soil Biology and Biochemistry* **40**, 515–527. doi:10.1016/j.soilbio.2007.09.019
- Aryal R, Kafley D, Beecham S, Morawska L (2018) Air quality in the Sydney metropolitan region during the 2013 blue mountains wildfire. *Aerosol and Air Quality Research* **18**, 2420–2432. doi:10.4209/aaqr. 2017.10.0427
- Baek S-J, Park A, Ahn Y-J, Choo J (2015) Baseline correction using asymmetrically reweighted penalized least squares smoothing. *The Analyst* 140, 250–257. doi:10.1039/c4an01061b
- Baldock JA, Skjemstad JO (2000) Role of the soil matrix and minerals in protecting natural organic materials against biological attack. *Organic Geochemistry* **31**, 697–710. doi:10.1016/S0146-6380(00)00049-8
- Barr C, Tibby J, Moss PT, Halverson GP, Marshall JC, McGregor GB, Stirling E (2017) A 25,000-year record of environmental change from Welsby Lagoon, North Stradbroke Island, in the Australian subtropics. *Quaternary International* **449**, 106–118. doi:10.1016/j. quaint.2017.04.011
- Bec KB, Grabska J, Bonn GK, Popp M, Huck CW (2020) Principles and applications of vibrational spectroscopic imaging in plant science: a review. *Frontiers in Plant Science* 11, 1226. doi:10.3389/fpls.2020. 01226
- Belcher CM, New SL, Santín C, Doerr SH, Dewhirst RA, Grosvenor MJ, Hudspith VA (2018) What can charcoal reflectance tell us about energy release in wildfires and the properties of pyrogenic carbon? *Frontiers in Earth Science* **6**, 169. doi:10.3389/feart.2018.00169
- Berna F, Behar A, Shahack-Gross R, Berg J, Boaretto E, Gilboa A, Sharon I, Shalev S, Shilstein S, Yahalom-Mack N, Zorn JR, Weiner S (2007) Sediments exposed to high temperatures: reconstructing pyrotechnological processes in Late Bronze and Iron Age Strata at Tel Dor (Israel). *Journal of Archaeological Science* 34, 358–373. doi:10.1016/j.jas.2006.05.011
- Black MP, Mooney SD, Haberle SG (2006) The fire, human and climate nexus in the Sydney Basin, eastern Australia. *Holocene* **17**, 469–480. doi:10.1177/0959683607077024

- Blarquez O, Girardin MP, Leys B, Ali AA, Aleman JC, Bergeron Y, Carcaillet C (2013) Paleofire reconstruction based on an ensemble-member strategy applied to sedimentary charcoal. *Geophysical Research Letters* **40**, 2667–2672. doi:10.1002/grl.50504
- Bradstock RA, Auld TD, ELLIS ME, Cohn JS (1992) Soil temperatures during bushfires in semi-arid, mallee shrublands. *Australian Journal of Ecology* **17**, 433–440. doi:10.1111/j.1442-9993.1992.tb00826.x
- Bradstock RA, Hammill KA, Collins L, Price O (2010) Effects of weather, fuel and terrain on fire severity in topographically diverse landscapes of south-eastern Australia. *Landscape Ecology* **25**, 607–619. doi:10.1007/s10980-009-9443-8
- Bronk Ramsey C (2009) Dealing with outliers and offsets in radiocarbon dating. *Radiocarbon* 51, 1023–1045. doi:10.1017/s0033822200034093
- Byram GM (1959) Combustion of Forest Fuels. In 'Forest fire: control and use'. (Ed. KP Davis) pp. 61–89. (McGraw-Hill: New York, NY, USA)
- Chalson JM, Martin HA (2009) A Holocene history of the vegetation of the Blue Mountains, New South Wales. *Proceedings of the Linnean Society of New South Wales* 130, 77–109.
- Chapple RS, Ramp D, Bradstock RA, Kingsford RT, Merson JA, Auld TD, Fleming PJS, Mulley RC (2011) Integrating science into management of ecosystems in the Greater Blue Mountains. *Environmental Management* **48**, 659–674. doi:10.1007/s00267-011-9721-5
- Chuvieco E, Congalton RG (1989) Application of remote sensing and geographic information systems to forest hazard mapping. *Remote Sensing of Environment* **29**, 147–159. doi:10.1016/0034-4257(89) 90023-0
- Clark JS (1988) Particle motion and the theory of charcoal analysis: source area, transport, deposition, and sampling. *Quaternary Research* **30**, 67–80. doi:10.1016/0033-5894(88)90088-9
- Conedera M, Tinner W, Neff C, Meurer M, Dickens AF, Krebs P (2009) Reconstructing past fire regimes: methods, applications, and relevance to fire management and conservation. *Quaternary Science Reviews* **28**, 555–576. doi:10.1016/j.quascirev.2008.11.005
- Constantine MIV, Mooney S, Hibbert B, Marjo C, Bird M, Cohen T, Forbes M, McBeath A, Rich A, Stride J (2021) Using charcoal, ATR FTIR and chemometrics to model the intensity of pyrolysis: exploratory steps towards characterising fire events. *Science of The Total Environment* **783**, 147052. doi:10.1016/j.scitotenv.2021.147052
- Constantine MIV, Zhu X, Cadd H, Mooney S (2023) Investigating the effect of oxidants on the quantification and characterization of charcoal in two southeast Australian sedimentary records. *Fire* **6**, 4–13. doi:10.3390/fire6020054
- Cortizas AM, López-Merino L, Silva-Sánchez N, Sjöström JK, Kylander ME (2021) Investigating the mineral composition of peat by combining FTIR-ATR and multivariate analysis. *Minerals* 11, 1084. doi:10.3390/min11101084
- Cowley KL, Fryirs KA, Hose GC (2016) Identifying key sedimentary indicators of geomorphic structure and function of upland swamps in the Blue Mountains for use in condition assessment and monitoring. *Catena* **147**, 564–577. doi:10.1016/j.catena.2016.08.016
- Cunningham CJ (1984) Recurring natural fire hazards: a case study of the Blue Mountains, New South Wales, Australia. *Applied Geography* **4**, 5–27. doi:10.1016/0143-6228(84)90002-X
- de Santana H, Toni LRM, Benetoli LO dB, Zaia CTBV, Rosa M, Zaia DAM (2006) Effect in glyphosate adsorption on clays and soils heated and characterization by FT-IR spectroscopy. *Geoderma* **136**, 738–750. doi:10.1016/j.geoderma.2006.05.012
- Dlapa P, Bodí MB, Mataix-solera J, Cerdà A, Doerr SH (2013) FT-IR spectroscopy reveals that ash water repellency is highly dependent on ash chemical composition. *Catena* **108**, 35–43. doi:10.1016/j.catena. 2012.02.011
- Dodson JR (1987) Mire development and environmental change, Barrington Tops, New South Wales, Australia. *Quaternary Research* **27**, 73–81. doi:10.1016/0033-5894(87)90050-0
- Dorez G, Ferry L, Sonnier R, Taguet A, Lopez-Cuesta JM (2014) Effect of cellulose, hemicellulose and lignin contents on pyrolysis and combustion of natural fibers. *Journal of Analytical and Applied Pyrolysis* **107**, 323–331. doi:10.1016/j.jaap.2014.03.017
- Dragovich D, Morris R (2002) Sediments and organic matter transfer following bushfires in the Blue Mountains, Australia. In 'The Structure, Function and Management Implication of Fluvial

- Sedimentary Systems. Proceedings of an international symposium'. Alice Springs, NT, Australia. pp. 325–331.
- El Atfy H, Havlik P, Krüger PS, Manfroi J, Jasper A, Uhl D (2017) Pre-Quaternary wood decay 'caught in the act' by fire–examples of plantmicrobe-interactions preserved in charcoal from clastic sediments. *Historical Biology* **31**, 952–961. doi:10.1080/08912963.2017. 1413101
- Ellerbrock R, Gerke HH, Bachmann J, Goebel M-O (2005) Composition of organic matter fractions for explaining wettability of three forest soils. *Soil Science Society of America Journal* **69**, 57-66. doi:10.2136/sssaj2005.0057
- Fang MX, Shen DK, Li YX, Yu CJ, Luo ZY, Cen KF (2006) Kinetic study on pyrolysis and combustion of wood under different oxygen concentrations by using TG-FTIR analysis. *Journal of Analytical and Applied Pyrolysis* 77, 22–27. doi:10.1016/j.jaap.2005.12.010
- Farmer VC (1974) 'The Infrared Spectra of Minerals.' Mineralogical Society Monograph 4, 331–363.
- Fernández I, Cabaneiro A, Carballas T (1997) Organic matter changes immediately after a wildfire in an Atlantic forest soil and comparison with laboratory soil heating. *Soil Biology and Biochemistry* **29**, 1–11. doi:10.1016/S0038-0717(96)00289-1
- Forbes M, Cohen T, Jacobs Z, Marx S, Barber E, Dodson J, Zamora A, Cadd H, Francke A, Constantine M, Mooney S, Short J, Tibby J, Parker A, Cendón D, Peterson M, Tyler J, Swallow E, Haines H, Gadd P, Woodward C (2021) Comparing interglacials in eastern Australia: a multi-proxy investigation of a new sedimentary record. *Quaternary Science Reviews* **252**, 106750. doi:10.1016/j.quascirev. 2020.106750
- Freidman BL, Fryirs KA (2015) Rehabilitating upland swamps using environmental histories: a case study of the Blue Mountains Peat Swamps, Eastern Australia. *Geografiska Annaler, Series A: Physical Geography* **97**, 337–353. doi:10.1111/geoa.12068
- Freund M, Henley BJ, Karoly DJ, Allen KJ, Baker PJ (2017) Multicentury cool- and warm-season rainfall reconstructions for Australia's major climatic regions. *Climate of the Past* 13, 1751–1770. doi:10.5194/cp-13-1751-2017
- Fryirs K, Freidman B, Williams R, Jacobsen G (2014) Peatlands in eastern Australia? Sedimentology and age structure of Temperate Highland Peat Swamps on Sandstone (THPSS) in the Southern Highlands and Blue Mountains of NSW, Australia. *Holocene* 24, 1527–1538. doi:10.1177/0959683614544064
- Fryirs KA, Cowley KL, Hejl N, Chariton A, Christiansen N, Dudaniec RY, Farebrother W, Hardwick L, Ralph T, Stow A, Hose G (2021) Extent and effect of the 2019-20 Australian bushfires on upland peat swamps in the Blue Mountains, NSW. *International Journal of Wildland Fire* **30**, 294–300. doi:10.1071/WF20081
- Gosling WD, Cornelissen HL, McMichael CNH (2019) Reconstructing past fire temperatures from ancient charcoal material. *Palaeogeography, Palaeoclimatology, Palaeoecology* **520**, 128–137. doi:10.1016/j.palaeo.2019.01.029
- Guénon R, Vennetier M, Dupuy N, Roussos S, Pailler A, Gros R (2013)
  Trends in recovery of Mediterranean soil chemical properties and
  microbial activities after infrequent and frequent wildfires. *Land*Degradation and Development 24, 115–128. doi:10.1002/ldr.1109
- Guo Y, Bustin RM (1998) FTIR spectroscopy and reflectance of modern charcoals and fungal decayed woods: implications for studies of inertinite in coals. *International Journal of Coal Geology* **37**, 29–53. doi:10.1016/S0166-5162(98)00019-6
- Haberhauer G, Rafferty B, Strebl F, Gerzabek MH (1998) Comparison of the composition of forest soil litter derived from three different sites at various decompositional stages using FTIR spectroscopy. *Geoderma* 83, 331–342. doi:10.1016/S0016-7061(98)00008-1
- Hahn A, Vogel H, Andó S, Garzanti E, Kuhn G, Lantzsch H, Schüürman J, Vogt C, Zabel M (2018) Using Fourier transform infrared spectroscopy to determine mineral phases in sediments. *Sedimentary Geology* **375**, 27–35. doi:10.1016/j.sedgeo.2018.03.010
- Hammill KA, Bradstock RA (2006) Remote sensing of fire severity in the Blue Mountains: influence of vegetation type and inferring fire intensity. *International Journal of Wildland Fire* **15**, 213–226. doi:10.1071/WF05051
- Hammill K, Tasker L, Barker C (2013) The Invisible Mosaic: Fire Regimes in One of NSW's Most Iconic Conservation Areas. In 'Proceedings from 9th Biennial NCCNSW Bushfire Conference'. p. 13

- Heinrich I, Banks JCG (2005) Dendroclimatological potential of the Australian red cedar. *Australian Journal of Botany* **53**, 21–32. doi:10.1071/BT04033
- Hogg AG, Heaton TJ, Hua Q, Palmer JG, Turney CSM, Southon J, Bayliss A, Blackwell PG, Boswijk G, Bronk Ramsey C, Pearson C, Petchey F, Reimer P, Reimer R, Wacker L (2020) SHCal20 Southern Hemisphere Calibration, 0-55,000 Years cal BP. *Radiocarbon* 62, 759–778. doi:10.1017/RDC.2020.59
- Hong H, Chen S, Fang Q, Algeo TJ, Zhao L (2019) Adsorption of organic matter on clay minerals in the Dajiuhu peat soil chronosequence, South China. Applied Clay Science 178, 105125. doi:10.1016/j.clay. 2019.105125
- Hua Q, Turnbull JC, Santos GM, Rakowski AZ, Ancapichún S, De Pol-Holz R, Hammer S, Lehman SJ, Levin I, Miller JB, Palmer JG, Turney CSM (2021) Atmospheric radiocarbon for the period 1950-2019. *Radiocarbon* **64**, 723–745. doi:10.1017/RDC.2021.95
- Huat BBK, Kazemian S, Prasad A, Barghchi M (2011) State of an art review of peat: general perspective. *International Journal of Physical Sciences* **6**, 1988–1996. doi:10.5897/JJPS11.192
- Kaal J, Schellekens J, Nierop KGJ, Martínez Cortizas A, Muller J (2014) Contribution of organic matter molecular proxies to interpretation of the last 55ka of the Lynch's Crater record (NE Australia). Palaeogeography, Palaeoclimatology, Palaeoecology 414, 20–31. doi:10.1016/j.palaeo.2014.07.040
- Keeley JE, Syphard AD (2016) Climate change and future fire regimes: examples from California. *Geosciences* **6**, 37. doi:10.3390/geosciences6030037
- Keiluweit M, Nico PS, Johnson M, Kleber M (2010) Dynamic molecular structure of plant biomass-derived black carbon (biochar). Environmental Science and Technology 44, 1247–1253. doi:10.1021/es9031419
- Knicker H, González-Vila FJ, Polvillo O, González JA, Almendros G (2005) Fire-induced transformation of C- and N- forms in different organic soil fractions from a Dystric Cambisol under a Mediterranean pine forest (*Pinus pinaster*). Soil Biology and Biochemistry 37, 701–718. doi:10.1016/j.soilbio.2004.09.008
- Kolka R, Sturtevant B, Townsend P, Miesel J, Wolter P, Fraver S, Desutter T (2014) Post-Fire comparisons of forest floor and soil carbon, nitrogen, and mercury pools with fire severity indices. Soil Science Society of America Journal 78, S58–S65. doi:10.2136/sssaj2013.08.0351nafsc
- Krull ES, Thompson CH, Skjemstad JO (2004) Chemistry, radiocarbon ages, and development of a subtropical acid peat in Queensland, Australia. *Australian Journal of Soil Research* **42**, 411–425. doi:10.1071/SR03144
- Kuhry P, Vitt DH (1996) Fossil carbon/nitrogen ratios as a measure of peat decomposition. Ecology 77, 271–275. doi:10.2307/2265676
- Lammers K, Arbuckle-Keil G, Dighton J (2009) FT-IR study of the changes in carbohydrate chemistry of three New Jersey pine barrens leaf litters during simulated control burning. *Soil Biology and Biochemistry* **41**, 340–347. doi:10.1016/j.soilbio.2008.11.005
- Lane PNJ, Sheridan GJ, Noske PJ, Sherwin CB (2008) Phosphorus and nitrogen exports from SE Australian forests following wildfire. *Journal of Hydrology* **361**, 186–198. doi:10.1016/j.jhydrol.2008. 07 041
- Leigh C, Bush A, Harrison ET, Ho SS, Luke L, Rolls RJ, Ledger ME (2015) Ecological effects of extreme climatic events on riverine ecosystems: insights from Australia. *Freshwater Biology* **60**, 2620–2638. doi:10.1111/fwb.12515
- Le Losq C (2018) 'Rampy: a Python library for processing spectroscopic (IR, Raman, XAS...) data.' (Zenodo)
- Lu S, Dosseto A, Lemarchand D, Dlapa P, Simkovic I, Bradstock R (2022) Investigating boron isotopes and FTIR as proxies for bushfire severity. *Catena* **219**, 106621. doi:10.1016/j.catena.2022.106621
- Lupascu M, Akhtar H, Smith TEL, Sukri RS (2020) Post-fire carbon dynamics in the tropical peat swamp forests of Brunei reveal long-term elevated CH<sub>4</sub> flux. *Global Change Biology* **26**, 5125–5145. doi:10.1111/gcb.15195
- Madejová J (2003) FTIR techniques in clay mineral studies. *Vibrational Spectroscopy* **31**, 1–10. doi:10.1016/S0924-2031(02)00065-6
- Maezumi SY, Gosling WD, Kirschner J, Chevalier M, Cornelissen HL, Heinecke T, McMichael CNH (2021) A modern analogue matching approach to characterize fire temperatures and plant species from

- charcoal. *Palaeogeography, Palaeoclimatology, Palaeoecology* **578**, 110580. doi:10.1016/j.palaeo.2021.110580
- Martín A, Díaz-Raviña M, Carballas T (2012) Short- and medium-term evolution of soil properties in Atlantic forest ecosystems affected by wildfires. *Land Degradation and Development* **23**, 427–439. doi:10.1002/ldr.1078
- Mastrolonardo G, Francioso O, Foggia M, Di, Bonora S, Forte C, Certini G (2015a) Soil pyrogenic organic matter characterisation by spectroscopic analysis: a study on combustion and pyrolysis residues. *Journal of Soil and Sediments* 15, 769–780. doi:10.1007/s11368-014-1034-x
- Mastrolonardo G, Rumpel C, Forte C, Doerr SH, Certini G (2015b) Abundance and composition of free and aggregate-occluded carbohydrates and lignin in two forest soils as affected by wildfires of different severity. *Geoderma* **245–246**, 40–51. doi:10.1016/j. geoderma.2015.01.006
- Mecozzi M, Pietrantonio E (2006) Carbohydrates proteins and lipids in fulvic and humic acids of sediments and its relationships with mucilaginous aggregates in the Italian seas. *Marine Chemistry* **101**, 27–39. doi:10.1016/j.marchem.2006.01.001
- Mooney S, Martin L, Goff J, Young ARM (2021) Sedimentation and organic content in the mires and other sites of sediment accumulation in the Sydney region, eastern Australia, in the period after the Last Glacial Maximum. *Quaternary Science Reviews* **272**, 107216. doi:10.1016/j.quascirev.2021.107216
- Nave LE, Vance ED, Swanston CW (2011) Fire effects on temperate forest soil C and N storage. *Ecological Applications* **21**, 1189–1201. doi:10.1890/10-0660.1
- Nedkov R, Molla I, Velizarova E, Radeva K (2018) Application of remote sensing data for forest fires severity assessment. In 'Earth Resources and Environmental Remote Sensing/GIS Application IX.'. (Eds U Michel, K Schulz) p. 10790U. (International Society for Optics and Photonics) doi:10.1117/12.2325742
- Nguyen BT, Lehmann J, Kinyangi J, Smernik R, Riha SJ, Engelhard MH (2008) Long-term black carbon dynamics in cultivated soil. *Biogeochemistry* **89**, 295–308. doi:10.1007/s10533-008-9220-9
- Orians GH, Milewski A V (2007) Ecology of Australia: the effects of nutrient-poor soils and intense fires. *Biological Reviews* **82**, 393–423. doi:10.1111/j.1469-185X.2007.00017.x
- Raison RJ, Khanna PK, Woods PV (1985) Mechanisms of element transfer to the atmosphere during vegetation fires. *Canadian Journal of Forest Research* **15**, 132–140. doi:10.1139/x85-022
- Rausa R, Mascolo G, Bassetti A (1999) Thermal treatment of sediments as a function of temperature and reacting atmosphere. *Journal of Analytical and Applied Pyrolysis* **52**, 115–135. doi:10.1016/S0165-2370(99)00054-6
- Ryan R, Dosseto A, Lemarchand D, Dlapa P, Thomas Z, Simkovic I, Bradstock R (2023) Boron isotopes and FTIR spectroscopy to identify past high severity fires. *Catena* **222**, 106887. doi:10.1016/j.catena. 2022.106887
- Santín C, Knicker H, Fernández S, Menéndez-Duarte R, Álvarez MÁ (2008) Wildfires influence on soil organic matter in an Atlantic mountainous region (NW of Spain). *Catena* **74**, 286–295. doi:10.1016/j.catena.2008.01.001
- Santín C, Doerr SH, Kane ES, Masiello CA, Ohlson M, de la Rosa JM, Preston CM, Dittmar T (2016) Towards a global assessment of pyrogenic carbon from vegetation fires. *Global Change Biology* **22**, 76–91. doi:10.1111/gcb.12985
- Sazawa K, Wakimoto T, Fukushima M, Yustiawati Y, Syawal MS, Hata N, Taguchi S, Tanaka S, Tanaka D, Kuramitz H (2018) Impact of peat fire on the soil and export of dissolved organic carbon in tropical peat soil, Central Kalimantan, Indonesia. *ACS Earth and Space Chemistry* **2**, 692–701. doi:10.1021/acsearthspacechem.8b00018
- Schmidt MWI, Noack AG (2000) Analysis, distribution, implications, and current challenges. *Global Biogeochemical Cycles* **14**, 777–793. doi:10.1029/1999GB001208
- Schroeder P (2002) Infrared spectroscopy in clay science. *Teaching Clay Science* 11, 182–206.
- Shakesby RA, Doerr SH (2006) Wildfire as a hydrological and geomorphological agent. *Earth-Science Reviews* **74**, 269–307. doi:10.1016/j.earscirev.2005.10.006

- Silva-Sánchez N, Martínez Cortizas A, Abel-Schaad D, López-Sáez JA, Mighall TM (2016) Influence of climate change and human activities on the organic and inorganic composition of peat during the 'Little Ice Age' (El Payo mire, W Spain). *Holocene* **26**, 1290–1303. doi:10.1177/0959683616638439
- Simkovic I, Dlapa P, Doerr SH, Mataix-Solera J, Sasinkova V (2008) Thermal destruction of soil water repellency and associated changes to soil organic matter as observed by FTIR spectroscopy. *Catena* 74, 205–211. doi:10.1016/j.catena.2008.03.003
- Smidt E, Eckhardt KU, Lechner P, Schulten HR, Leinweber P (2005) Characterization of different decomposition stages of biowaste using FT-IR spectroscopy and pyrolysis-field ionization mass spectrometry. *Biodegradation* 16, 67–79. doi:10.1007/s10531-004-0430-8
- Tasker E, Hammill K (2011) Fire Regimes and Vegetation in the Greater Blue Mountains World Heritage Area. In 'Proceedings of Bushfire CRC and AFAC 2010 Conference Science Day.' pp. 182–195. Thomas AD, Walsh RPD, Shakesby RA (1999) Nutrient losses in eroded
- Thomas AD, Walsh RPD, Shakesby RA (1999) Nutrient losses in eroded sediment after fire in eucalyptus and pine forests in the wet Mediterranean environment of northern Portugal. *Catena* **36**, 283–302. doi:10.1016/S0341-8162(99)00051-X
- Timbal B, Fawcett R (2013) A historical perspective on Southeastern Australian rainfall since 1865 using the instrumental record. *Journal of Climate* **26**, 1112–1129. doi:10.1175/JCLI-D-12-00082.1
- Turney C, Becerra-Valdivia L, Sookdeo A, Thomas ZA, Palmer J, Haines HA, Cadd H, Wacker L, Baker A, Andersen MS, Jacobsen G, Meredith K, Chinu K, Bollhalder S, Marjo C (2021) Radiocarbon protocols and first intercomparison results from the Chronos <sup>14</sup>Carbon-Cycle Facility, University of New South Wales, Sydney, Australia. *Radiocarbon* **63**, 1003–1023. doi:10.1017/RDC.2021.23
- van der Werf GR, Randerson JT, Giglio L, Van Leeuwen TT, Chen Y, Rogers BM, Mu M, Van Marle MJE, Morton DC, Collatz GJ, Yokelson RJ, Kasibhatla PS (2017) Global fire emissions estimates during 1997-2016. *Earth System Science Data* **9**, 697–720. doi:10.5194/essd-9-697-2017
- Wang G, Cai W (2020) Two-year consecutive concurrences of positive Indian Ocean Dipole and Central Pacific El Niño preconditioned the 2019/2020 Australian "black summer" bushfires. *Geoscience Letters* 7, 19. doi:10.1186/s40562-020-00168-2
- Whight S, Bradstock R (1999) Indices of fire characteristics in sandstone heath. *International Journal of Wildland Fire* 9, 145–153. doi:10.1071/WF00012
- Williams RJ, Bradstock RA, Cary GJ, Enright NJ, Gilll MA, Leidloff AC, Lucas C, Whelan R, Andersen AN, Bowman DMJS, Clarke PJ, Cook GD, Hennessy K, York A (2009) Interactions between climate change, fire regimes and biodiversity in Australia a preliminary assessment. Vol. 17. pp. 1–196. (Report to the Department of Climate Change and Department of the Environment, Heritage and Arts: Canberra, Australia)
- Wu Y, Zhang N, Slater G, Waddington JM, de Lannoy CF (2020) Hydrophobicity of peat soils: characterization of organic compound changes associated with heat-induced water repellency. *Science of The Total Environment* **714**, 136444. doi:10.1016/j.scitotenv.2019. 136444
- Yang H, Yan R, Chen H, Lee DH, Zheng C (2007) Characteristics of hemicellulose, cellulose and lignin pyrolysis. *Fuel* **86**, 1781–1788. doi:10.1016/j.fuel.2006.12.013
- Yusiharni E, Gilkes R (2012) Rehydration of heated gibbsite, kaolinite and goethite: an assessment of properties and environmental significance. Applied Clay Science 64, 61–74. doi:10.1016/j.clay.2011.12.005
- Zaccone C, Rein G, D'Orazio V, Hadden RM, Belcher CM, Miano TM (2014) Smouldering fire signatures in peat and their implications for palaeoenvironmental reconstructions. *Geochimica et Cosmochimica Acta* 137, 134–146. doi:10.1016/j.gca.2014.04.018
- Zanelli R, Egli M, Mirabella A, Abdelmoula M, Plötze M, Nötzli M (2006) 'Black' soils in the southern Alps: clay mineral formation and transformation, x-ray amorphous Al phases and Fe forms. *Clays and Clay Minerals* **54**, 703–720. doi:10.1346/CCMN.2006.0540606
- Collins L, Bradstock RA, Penman TD (2014) Can precipitation influence landscape controls on wildfire severity? A case study within temperate eucalypt forests of south-eastern Australia. *International Journal of Wildland Fire* 23(1), 9. doi:10.1071/wf12184

Data availability. Data will be made available upon request.

Conflicts of interest. The authors declare no conflicts of interest.

Declaration of funding. Funding was provided by ARC Discovery Grant DP200101123. Support from the grant SGA VEGA 1/0703/23 is also appreciated.

Acknowledgements. We thank NPWS for permitting site access and sample collection. Funding was provided by ARC Discovery Grant DP200101123. Support from the grant SGA VEGA 1/0703/23 is also appreciated. RR acknowledges an APA PhD scholarship and a top-up scholarship from Natural Hazards Research Australia. We also thank Mark Constantine, Mark Quoyle, Maame Adowa Maisie, and Xiaohong Zhu for their help in the field. We thank the anonymous peer reviewers and the editors, Prof. Stefan Doerr, and Dr. Alison Bentley for their feedback on this manuscript.

#### **Author affiliations**

^Wollongong Isotope Geochronology Laboratory, School of Earth, Atmospheric and Life Sciences, University of Wollongong, NSW 2522, Australia.

<sup>B</sup>Centre for Environmental Risk Management of Bushfires, Institute for Conservation Biology and Management, University of Wollongong, Wollongong, NSW 2522, Australia.

<sup>C</sup>Department of Soil Science, Faculty of Natural Sciences, Comenius University, Mlynská dolina B-2, 842 15 Bratislava, Slovak Republic.

<sup>D</sup>Chronos 14Carbon-Cycle Facility, Mark Wainwright Analytical Centre, University of New South Wales, NSW 2052, Australia.

ESchool of Geography and Environmental Science, University of Southampton, Southampton, SO17 1BJ, United Kingdom.

FEarth and Sustainability Science Research Centre, UNSW Sydney, NSW 2052, Australia.